Palaeogeography, Palaeoclimatology, Palaeoecology 418 (2015) 75–89

Contents lists available at ScienceDirect

Palaeogeography, Palaeoclimatology, Palaeoecology

journal homepage: www.elsevier.com/locate/palaeo

Challenging the sensitivity limits of Paleomagnetism: Magnetostratigraphy of weakly magnetized Guadalupian–Lopingian (Permian) Limestone from Kyushu, Japan

Joseph L. Kirschvink [a,b,*], Yukio Isozaki [c], Hideotoshi Shibuya [d], Yo-ichiro Otofuji [e], Timothy D. Raub [f], Isaac A. Hilburn [a], Teruhisa Kasuya [c], Masahiko Yokoyama [e], Magali Bonifacie [g]

[a] Division of Geological & Planetary Sciences, California Institute of Technology 170-25, Pasadena, CA 91125, USA
[b] Earth-Life Science Institute, Tokyo Institute of Technology, Meguro, Tokyo 152-8550, Japan
[c] Dept. Earth Sci. Astron., Univ. Tokyo, Meguro, Tokyo 153-8902, Japan
[d] Dept. Earth & Env. Sci., Kumamoto Univ., Kumamoto 860-8555 Japan
[e] Dept. Earth Planet. Sci., Kobe Univ., Kobe 657-8501, Japan
[f] Dept. of Earth Sciences, University of St Andrews, St Andrews, KY16 9AL Scotland UK
[g] Institut de Physique du Globe de Paris, Laboratoire Géochimie des Isotopes Stables, IPGP, Bureau 515, rue Jussieu, 75238 Paris cedex 05, France

ARTICLE INFO

Article history:
Received 5 July 2014
Received in revised form 14 October 2014
Accepted 28 October 2014
Available online 4 November 2014

Keywords:
Paleomagnetism
Limestone
Permian
Kiaman superchron
Illawarra Reversal
Mass extinction

ABSTRACT

Despite their utility for bio- and chemostratigraphy, many carbonate platform sequences have been difficult to analyze using paleomagnetic techniques due to their extraordinarily weak natural remanent magnetizations (NRMs). However, the physical processes of magnetization imply that stable NRMs can be preserved that are many orders of magnitude below our present measurement abilities. Recent advances in reducing the noise level of superconducting magnetometer systems, particularly the introduction of DC-SQUID sensors and development of a low-noise sample handling system using thin-walled quartz-glass vacuum tubes, have solved many of these instrumentation problems, increasing the effective sensitivity by a factor of nearly 50 over the previous techniques of SQUID moment magnetometry.

Here we report the successful isolation of a two-polarity characteristic remanent magnetization from Middle–Late Permian limestone formed in the atoll of a mid-oceanic paleo-seamount, now preserved in the Jurassic accretionary complex in Japan, which had proved difficult to analyze in past studies. Paleothermometric indicators including Conodont Alteration Indices, carbonate petrology, and clumped isotope paleothermometry are consistent with peak burial temperatures close to 130 °C, consistent with rock magnetic indicators suggesting fine-grained magnetite and hematite holds the NRM. The magnetic polarity pattern is in broad agreement with previous global magnetostratigraphic summaries from the interval of the Early–Middle Permian Kiaman Reversed Superchron and the Permian–Triassic mixed interval, and ties the Tethyan–Panthalassan fusuline zones to it. Elevated levels of hematite associated with the positive $\delta^{13}C_{carb}$ of the Kamura event argue for a brief spike in environmental oxygen. The results also place the paleo-seamount at a paleolatitude of ~12° S, in the middle of the Panthalassan Ocean, and imply a N/NW transport toward the Asian margin of Pangea during Triassic and Jurassic times, in accordance with the predicted trajectory from its tectono-sedimentary background. These developments should expand the applicability of magnetostratigraphic techniques to many additional portions of the Geological time scale.

1. Introduction

A fundamental goal of stratigraphy is to establish interbasin correlations with globally-isochronous time horizons, including the critical stratotype horizons, and to correlate these to the magnetic reversal patterns of the Geomagnetic Reversal Time Scale (GRTS), which should be essentially isochronous on a global scale. Most of the global stratotype sections and points (GSSPs) have been defined in fossiliferous, shallow marine carbonate platform sequences due to their proven ability to record pristine biological and geochemical records of Earth history. Unfortunately, it is well known that biostratigraphically-defined zone boundaries are often diachronous, and local oceanographic and geological effects can influence geochemical proxies for chemostratigraphic correlation.

* Corresponding author at: Division of Geological & Planetary Sciences, California Institute of Technology 170-25, Pasadena, CA 91125, USA. Tel.: +1 626 395 6136.
E-mail address: Kirschvink@caltech.edu (J.L. Kirschvink).

http://dx.doi.org/10.1016/j.palaeo.2014.10.037
0031-0182/

Efforts to use paleomagnetic techniques for unraveling magnetic polarity patterns in many GSSPs, however, have often proven frustrating. Prominent examples include the original definition of the Silurian–Devonian stratotype at Klonk, in the Czech Republic, where the metamorphic grade appears to have been too high to retain primary paleomagnetism (Ripperdan, 1990), and several Ordovician GSSPs on Anticosti Island, Canada (Ripperdan, 1990; Seguin and Petryk, 1986), where many of the pale carbonates were found to be too weakly magnetized to measure and demagnetize reliably using the conventional techniques of 25 years ago. From these studies it was simply not known whether the rocks had concentrations of magnetic minerals too small to produce a measureable moment, or if diagenetic processes and hydrocarbon migration had destroyed those that were there initially.

It has long been known that the physical processes of aligning magnetic minerals during the formation of sedimentary rocks can preserve stable magnetic components that are many orders of magnitude below the measurement ability of the best superconducting rock (moment) magnetometers (Kirschvink, 1981), even those using the enhanced sensitivity of DC-biased superconducting quantum interference devices (DC-SQUIDs) (Weiss et al., 2001). In fact, the situation is much worse than this sensor noise limit, as the intrinsic magnetic moment of most of the sample holders used in paleomagnetic studies (background noise) is typically several orders of magnitude higher than the sensor limit. DC-SQUID sensors in the commercially available 2G Enterprises™ rock magnetometers typically have r.m.s. magnetic moment noise levels of a few tenths of a pAm^2 (a few $\times 10^{-10}$ emu), whereas most sample holders measure at a few tens of pAm^2 (10^{-7} emu), several orders of magnitude higher. Recently, the introduction of acid-washed, thin-walled quartz-glass tubing for supporting samples with a vacuum has lowered this noise greatly by minimizing the amount of extraneous matter in the sense region of the SQUID magnetometers (Kirschvink et al., 2008). Coupled with a computer-controlled pick-and-place sample changing system, this permits the large numbers of precise demagnetization experiments needed for magnetostratigraphic studies to be performed rapidly.

We chose the Middle–Late Permian limestone from Kamura in Kyushu, Japan, to test the suitability of these new sample-measuring techniques because previous rock magnetic work (Yokoyama et al., 2007) demonstrated that these rocks contained fine-grained magnetite and hematite, but in concentrations making the NRM difficult to analyze. Most of the Jurassic accretionary complex in SW Japan that contains exotic Permian limestone blocks suffered at most lower greenschist facies metamorphism around 140 Ma (Isozaki et al., 1990), usually characterized by the mineral paragenesis of pumpellyite–actinolite, except some locally baked domains in close contact with the Cretaceous–Paleogene granitic intrusions. Although the Kamura area in central Kyushu is located near an active volcanic region, there are ample indications from the local geology that these rocks were never affected significantly by thermochemical alteration. The studied interval straddles the Middle–Late Permian boundary (Isozaki and Ota, 2001; Ota and Isozaki, 2006) and thus records the end-Guadalupian mass extinction event (Jin et al., 1994; Stanley and Yang, 1994) and possibly the top of the Kiaman Reversed Superchron, known as the 'Illawarra Reversal' (Cottrell et al., 2008; Courtillot and Olson, 2007; Gialanella et al., 1997; Gradstein et al., 2012; Irving, 1964; Isozaki, 2009; Opdyke et al., 2000), offering the possibility of enhancing the correlation between the two time scales. In particular, the first appearance of a solid Normal interval is critical in identifying the Illawarra Reversal that is expected within Wordian (Middle Guadalupian) time.

Application of these new techniques to the Kamura limestone reveals the presence of a stable, 2-polarity characteristic NRM that is broadly consistent with past studies of the geomagnetic polarity chronology for late Permian Time, including the top of the Kiaman Superchron. The characteristic direction, and the match to the reversal chronology, indicates that the Kamura atoll was located at about 12° South latitude in the Panthalassic Ocean. A minimum of 3000 km of N/NW transport would have been required for it to dock against the Eastern margin of Pangea during Jurassic time. The present result also has profound implications to the bio- and chemostratigraphic correlation between the mid-superoceanic paleo-atoll limestone and continental shelf carbonates around Pangea.

2. Geological setting

2.1. Tectono-sedimentary background

The Permian and Triassic limestone at Kamura (Takachiho town, Miyazaki prefecture; Fig. 1) in Kyushu forms a part of an ancient mid-oceanic atoll complex primarily developed on a mid-oceanic paleo-seamount (Isozaki, 2014; Isozaki and Ota, 2001; Kasuya et al., 2012; Ota and Isozaki, 2006; Sano and Nakashima, 1997). This limestone occurs as a several kilometer-long, lensoid allochthonous block within the Middle–Upper Jurassic disorganized mudstone/sandstone of the Jurassic accretionary complex in the Chichibu belt, southwest Japan, with remarkably little internal deformation (Fig. 2). The orientation of the late Paleozoic to early Mesozoic subduction zone beneath the Asian blocks (Isozaki, 1997a,b) implies that the seamount originated to the east (Pacific side) with respect to Asia, i.e., somewhere in the superocean Panthalassa, and accreted to the Asian margin in the Jurassic, approximately 100 million years later. The limestone blocks in the Kamura area retain parts of the primary mid-oceanic stratigraphy (ca. 135 m in thickness), and range from Wordian (middle Guadalupian) to Norian (Upper Triassic) time with several sedimentary breaks in the Triassic part (Isozaki, 2014; Kambe, 1963; Kanmera and Nakazawa, 1973; Kasuya et al., 2012; Koike, 1996; Ota and Isozaki, 2006).

2.2. Lithostratigraphy and paleoenvironments

The Iwato Formation consists of ca. 100 m-thick, dark gray to black bioclastic limestone. Bioclasts include fragments of bivalves, calcareous algae, crinoids, fusulines and other small foraminifera, indicating Guadalupian age. The lower part of the Iwato Formation comprises wackestone with a black, organic-rich matrix and yields abundant large bivalves (Family Alatoconchidae) and large-tested fusulines (e.g., *Neoschwagerina, Yabeina, Lepidolina*). The upper part comprises peloidal wackestone. Black organic matter probably of microbial origin is concentrated in peloids. Megafossils are absent in this interval, except for very rare rugose coral (*Liangshanophyllum*) from the uppermost part. All black limestones are free from dolomitization.

The overlying Mitai Formation consists of nearly 40 m-thick, light gray bioclastic dolomitic limestone. Bioclasts are derived from calcareous algae, crinoids, ostracodes, gastropods, bivalves, crinoids, brachiopods, coral, fusulines and small foraminifera of the Tethyan affinity, and indicate Lopingian age. The limestones are mostly grainstone/wackestone with lesser amounts of lime–mudstone that are fossiliferous, mostly massive, partly including 1 cm-thick, continuous to discontinuous bands with concentrations of peloids and algae. Crystals of secondary dolomite are generally concentrated around bioclasts (and avoided in the paleomagnetic sampling). The lowermost 1 m-thick bed is characterized by white bands containing abundant dolomitized dasycladacean algae.

All the Tethyan fusuline assemblages and associated fossils from the Iwato and Mitai formations indicate that the seamount was located in a low-latitude domain in the superocean Panthalassa under a tropical climate (Isozaki, 2006, 2014; Isozaki and Aljinovic, 2009; Kasuya et al., 2012).

2.3. Bio- and chemostratigraphy

Conodonts, the index fossils with the highest resolution for the Permian, have unfortunately not been found in the Permian Iwato and Mitai formations where our paleomagnetic samples come from, as the sedimentary facies was too shallow to host conodont animals. Fusulines are the most abundant among fossils, and they provide a basis for

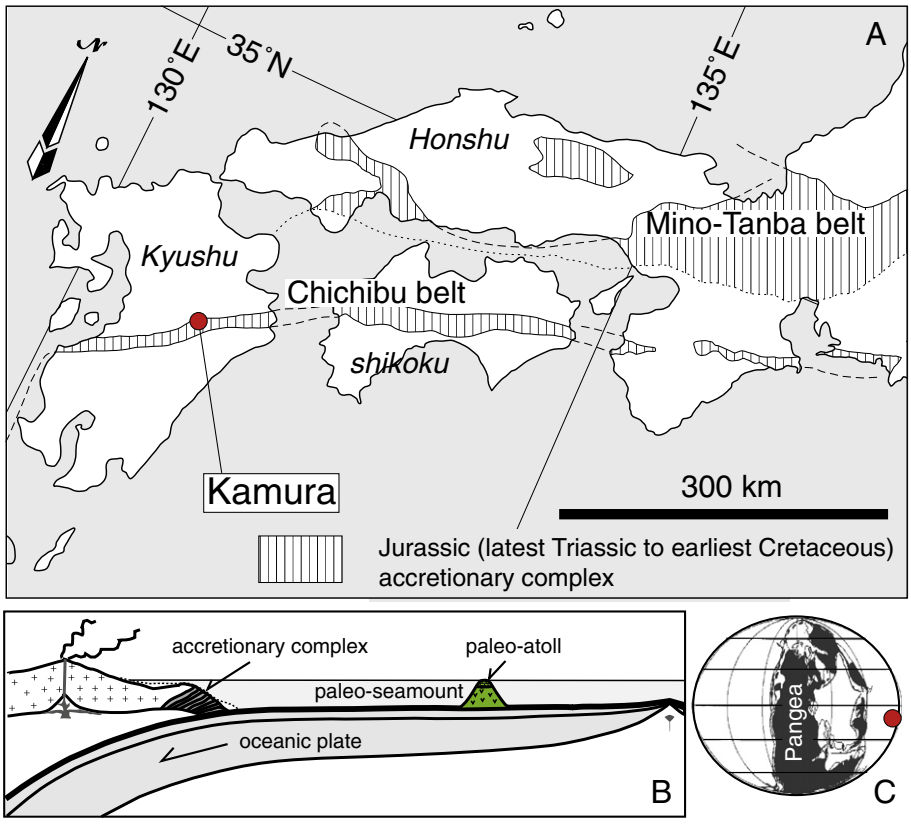

Fig. 1. (A) Index map of southwest Japan, showing the distribution of the Jurassic accretionary complex with accreted paleo-atoll limestones of the Chichibu belt, extending from central Kyushu, onto Shikoku and western Honshu. (B) A simplified cartoon of the paleo-ridge-arc transect interpreted to have been operating from Late Permian through mid-Jurassic time. (C) Paleogeography of the Permian world with the probable location of the Kamura seamount (filled circle). Adapted from Kasuya et al. (2012).

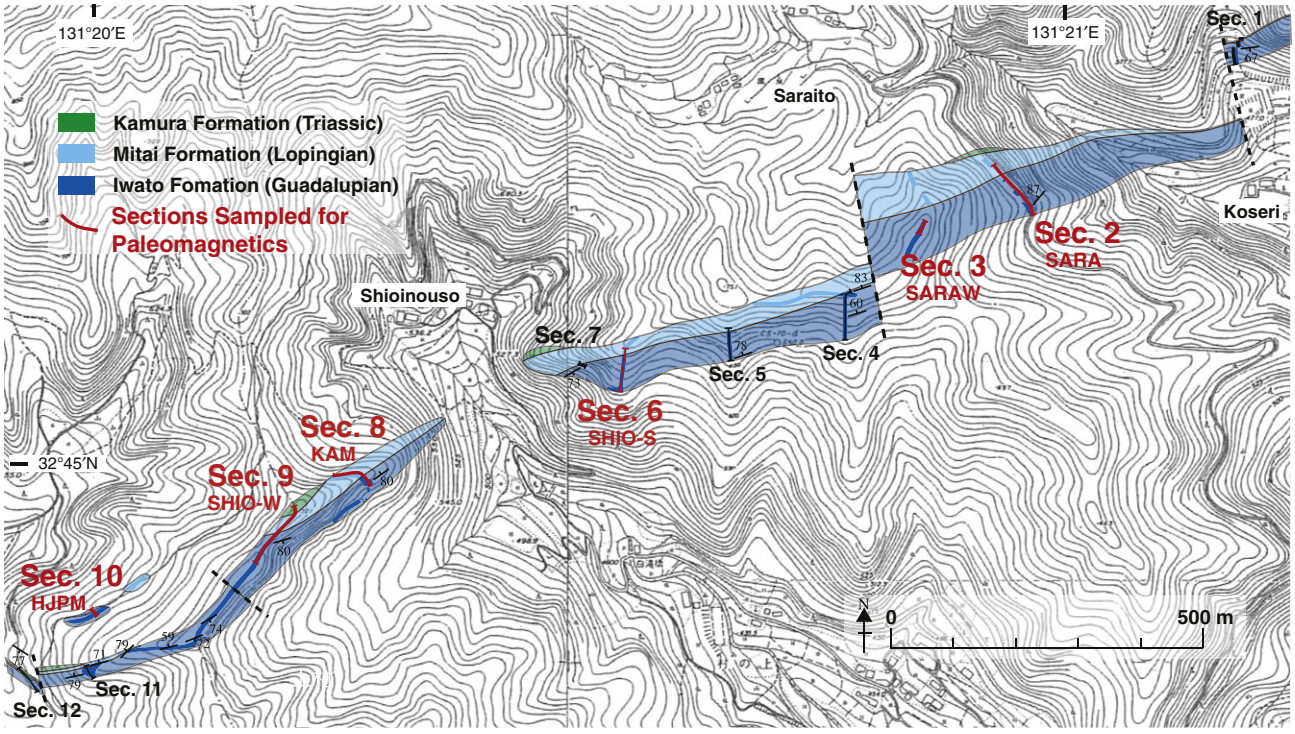

Fig. 2. Geological sketch map of the Kamura area in central Kyushu, showing the sections analyzed for paleomagnetics and the distribution of the Permo–Triassic paleo-atoll limestone sections. This figure is adapted from Kasuya et al. (2012). Beds within the exposure are nearly vertical to slightly overturned, striking generally ENE/WSW, and younging to the North.

subdividing the Iwato Formation into the following 5 biostratigraphic units; i.e., the *Neoschwagerina craticulifera* Zone, *Neoschwagerina margaritae* Zone, *Yabeina* Zone, *Lepidolina* Zone, and a barren interval, in ascending order (Kasuya et al., 2012; Ota and Isozaki, 2006). Stratigraphic positions of the zone boundaries are constrained by fossil occurrence to be better than 1 m, except for the *N. craticulifera*/*N. margaritae*, boundary which is estimated to be ~±5 m. The *N. craticulifera* Zone and *N. margaritae* Zone are correlated with the Wordian of Texas and with the Murgabian and lower Midian in Transcaucasia, whereas the *Yabeina* Zone and *Lepidolina* Zone, and most of the barren interval are correlated with the Capitanian (Upper Guadalupian) of Texas and with the middle–upper Midian in Transcaucasia (e.g., (Wardlaw et al., 2004)). The carbon isotope stratigraphy of the *Lepidolina* Zone and barren interval (Isozaki, 1997a,b) documented the occurrence of high positive plateau in $\delta^{13}C_{carb}$ values (>5‰) that can be correlated with the Capitanian rocks in North America and the European Tethys (e.g. (Isozaki et al., 2011)). In addition, the uniquely low Sr/Sr ratios (<0.7070) detected in the same interval also support the age assignment of the Capitanian (Kani et al., 2008; Kani et al., 2013).

The overlying Mitai Formation belongs to the *Codonofusiella–Reichelina* Zone that corresponds to the Wuchiapingian (Lower Lopingian) in South China. The carbon isotope stratigraphy also confirmed that the gradual positive excursion in the lowermost *Codonofusiella–Reichelina* Zone (Isozaki et al., 2007b) corresponds to the same signal detected in the *Clarkina dukoensis* Zone (lower Wuchiapingian) at Penglaitan, the GSSP (Global Stratotype Section and Point) of G–L boundary in South China (Chen et al., 2011; Wang et al., 2004).

2.4. Geochemistry

In terms of total organic content (TOC), the black limestone of the Iwato Formation varies between 0.13 and 0.77 wt.%, whereas the light gray dolomitic limestone of the Mitai Formation varies from 0.0044 to 0.0067 wt.% (Isozaki et al., 2007b), values which are typical of oceanic atoll environments. However, the carbonates in the Wordian to lower Capitanian interval at Kamura record a major excursion in the value of $\delta^{13}C_{carb}$, increasing from a stable value of ~+4.5‰ and reaching a maximum of ~+7.0‰ within the *Yabeina* Zone (fusuline) of the early–middle Capitanian. Thus the total duration of the Kamura event is estimated ca. 3–4 million years, occupying the majority of Capitanian time (Isozaki et al., 2007a).

In addition to the positive excursion in carbon isotopes, the Kamura limestones also preserve a record of the Paleozoic minimum in marine $^{87}Sr/^{86}Sr$ ratio, which reaches its nadir (0.706914 ± 0.000012) in late Capitanian time, essentially coincident with the Kamura isotope excursion (Kani et al., 2008).

2.5. Constraints on burial metamorphism

Although the Kamura limestone unit we have studied is a coherent block that crops out over a large area (~10 km long, ~150 meter thick, with bedding nearly vertical, and remarkably similar structural attitudes), it occurs as large exotic blocks within the younger Jurassic sandstone/mudstone along the length of the accretionary complex shown in Fig. 1 (Ota and Isozaki, 2006). It has long been known that limestone 'knockers' scraped off of subducting slabs often escape significant burial metamorphism under these conditions, as exemplified by the classic paleomagnetic study of the Laytonville Limestone in the Franciscan complex of central California (Alvarez et al., 1980). The sequence in Kyushu, however, has been intruded subsequently by felsic intrusions of arc affinity, and is in the vicinity of Mt. Aso, a major modern eruptive center on the island of Kyushu that is capable of producing local and/or regional thermochemical alteration. Paleomagnetic studies of Mesozoic rocks in both Kyushu and central Honshu sometimes show a complex pattern of remagnetization, indicating both thermal and chemical events have operated in some areas (Abrajevitch et al., 2011; Abrajevitch and Kodama, 2009; Ando et al., 2001; Kodama and Takeda, 2002; Oda and Suzuki, 2000; Shibuya and Sasajima, 1986; Uno et al., 2012).

Despite this, three observations suggest that the rocks that we are studying have not been altered to levels capable of erasing completely their initial remanent magnetizations. First, the shells of the giant bivalves appear remarkably pristine. They are built with a typical molluscan double-layered structure, where the external layer is composed of parallel-aligned prismatic calcite with c-axis perpendicular to the shell surface, whereas the inner layer is a micro-crystalline mosaic (Isozaki, 2006; Isozaki and Aljinovic, 2009). This textural difference argues against thermochemical alteration high enough to trigger the pervasive recrystallization of the carbonate, and certainly well below any carbonate decomposition temperature.

Second, conodonts in the overlying Triassic portions of the block are often preserved with Conodont Alteration Indices (CAI) as low as 2 on the scale of Epstein et al. (1977), implying only mild heating (60°–140 °C) on geological time scales, but peak heating of up to ~500 °C on the time scale of less than an hour (which is implausible in the geological setting of these rocks), (Ripperdan, 1990). Hence, a blanket, regional heating capable of complete remagnetization of the sediments can be ruled out, particularly as the most likely magnetic carriers (magnetite and hematite) are stable to much higher temperatures.

Unfortunately, conodonts have not been found in the Permian portion of the limestone in Kamura where our paleomagnetic samples come from, so their CAI values cannot be used to test for more significant thermochemical alteration from local intrusions or volcanic vents. However, field observations of localities where intrusions do impinge on the limestone reveal intense and visually obvious bleaching of the rock as the kerogens are destroyed. Our paleomagnetic sampling has avoided these areas. Further constraints from clumped isotope analyses are presented in Section 5.3 below.

3. Studied sections and rock samples

We studied 3 major sections in the Kamura area; i.e., Sections 2, 8, and 10 (Figs. 2, 3) with additional samples from 3 other sections (Section 4, 7, and 9; see Kausya et al. (2012) for details). Section 2, which crops out at the southeast of Saraito village (32° 45′12″ N, 131° 20′55″ E), contains 57 m of black limestone that belongs to the *N. craticulifera* Zone (Isozaki, 2006; Isozaki et al., 2007a; Kambe, 1963). Owing to the outcrop condition, we only sampled from the lower half of the section. Section 8 at the west of Shioinouso village (32° 44′58″ N, 131° 20′02″ E) contains 35 m of similar limestone that contains the upper Iwato Formation and the lower Mitai Formation, and spans the Guadalupian–Lopingian boundary (G–LB) as originally described by Ota and Isozaki (2006). We collected samples from the Capitanian *Lepidolina* Zone, overlying barren interval, and the Wuchiapingian *Codonofusiella–Reichelina* Zone. Section 10 at Hijirikawa consists of 9 m of thick black limestone of the Iwato Formation that belongs to the *Yabeina* Zone (Isozaki et al., 2007b). We collected samples from the entire section. As to the other 3 sections, Section 4 belongs to the *Neoschwagerina margaritae* Zone, whereas Sections 7 and 9 belong to the *Yabeina* Zone (Kasuya et al., 2012). Although there is no single continuous section that covers the entire Guadalupian stratigraphy in this area, we managed to collect samples from all fusuline zones ranging from the Wordian to Wuchiapingian, and in particular, at the continuous Section 8 that preserves a 35 m-thick limestone across the G–LB.

For the magnetostratigraphic study, we collected a total of 117 oriented core samples (2.5 cm diameter cylinders) of fine-grained limestone (lime mudstone composed of pure carbonates with scarce terrigenous components) from the above-described 3 sections in the Kamura area (Sections 2, 8 and 10), using standard magnetic and solar compass techniques. In addition, eleven hand samples from Sections 4, 7 and 9, in locations difficult to use the portable drills, were oriented *in-situ* using a

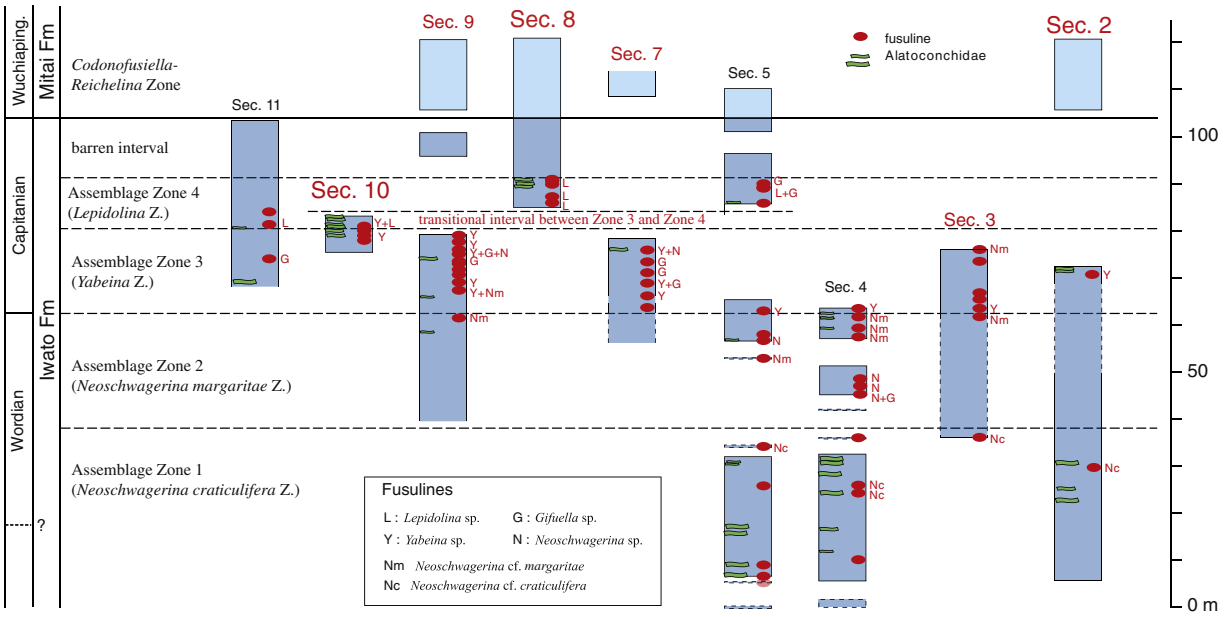

Fig. 3. Biostratigraphic correlation based on Fusuline zones for the localities sampled in the Kamura area. The section numbers correspond to those shown in Fig. 2. Assemblage zones 1–4 correspond to the standard Tethyan nomenclature.

custom magnetic and sun-compass system and removed for sample preparation in the laboratory. Forty additional block samples for intensive rock magnetic investigation were collected from Section 8 in the Capitanian and Wuchiapingian parts.

4. Materials & methods

4.1. Samples for paleomagnetic measurements

In the laboratory, the core samples were trimmed into as many 1-cm high flat-ended discs as possible using non-magnetic saw blades, and the innermost specimens from each core (furthest from surface weathering) were selected for initial measurement processes. Similar cores were drilled from the eleven oriented hand samples using a drill press setup, with between 1 and 3 cores per sample, and were reoriented and labeled using standard techniques. Oriented end chips from a representative batch of the cores from each locality were set aside for intensive rock magnetic analyses.

Due to the extremely weak magnetizations reported for these rocks by Yokoyama et al. (2007), we adopted moderately stringent clean-lab handling processes to minimize the possibility of stray ferromagnetic materials becoming attached to the rock surfaces during the measurement and demagnetization procedures. First, after cutting and trimming the samples with the diamond-impregnated drills and saw blades, and enhancing the fiducial orientation line with a diamond scribe, they were dipped vigorously but briefly (for less than 1 s) in concentrated, reagent-grade (12 N) HCl using plastic tongs, and then rinsed quickly in a large volume of deionized, fresh water. This acid treatment caused an immediate reaction with the surface carbonate on the samples, noticeably darkened the rock surface, and often left an oily, black residue floating on the surface of the cleaning liquids. Care had to be taken not to lose either the fiducial marks or the sample identification labels during this process. Next, specimens were labeled with a non-magnetic white, thermally-resistant ink, and were moved into the magnetically-shielded environment (<200 nT) surrounding the SQUID magnetometer work area for at least several days prior to measurement. The specimens, and all surfaces that touched them, were dusted off with high-pressure air that was passed through a 0.2 micron particulate filter prior to every measurement. We used disposable dust-free plastic gloves for handling all of the samples once the demagnetization procedures were started.

4.2. Paleomagnetism

All remanence measurements for this study were conducted on the Eugene M. Shoemaker Memorial Magnetometer, which is a 2G™ Enterprises model 755 superconducting rock magnetometer with 3-axis DC SQUIDS housed in a double-layer, mu-metal shielded room at Caltech. Sham measurements of the baseline noise on the system (run with everything operating except the quartz-glass vacuum sample holder) yield a repeatable threshold moment sensitivity of a few by 10^{-10} emu (~10^{-13} Am^2). Inclusion of the quartz-glass sample tubes (19 mm diameter with 1 mm thick walls) usually raised the baseline holder moment up by a factor of 10 to 100 above this, which is far too high for successfully measuring the set of Kamura limestone samples we were investigating. To knock down the moment of the sample holders, we first washed the tubes thoroughly with laboratory glass cleaners, and then soaked one end in reagent-grade, 12 N HCl for several days to dissolve any ferric contaminants on and/or within the glass that could be reached by the acid. For about a quarter of the glass tubes, this treatment resulted in holder moments below about 10^{-9} emu (10^{-12} Am^2 = 1 pAm^2). On occasion they could become magnetically 'invisible', consistently reaching down to the background noise level of the DC SQUID sensors. In addition, we implemented a routine in the RAPID software that allows the empty sample holder to be cleaned with maximum strength alternating-field (AF) demagnetization after every set of nine measurements.

To place this in context, we note that our standard specimen size (cylinders ~2.54 cm in diameter, by ~1 cm high) is about 40% smaller than the standard sample size traditionally used in most paleomagnetic laboratories (e.g., (Butler, 1992)). We did this because the smaller specimen volume allows twice as many samples to be put into the magnetically-shielded furnaces for thermal demagnetization (up to ~80 specimens per load), doubling the measurement rate. It also reduced the problem of jamming on early versions of the automatic sample changer used by the RAPID consortium (Kirschvink et al., 2008). Note that we prefer to discuss sensitivity in terms of *magnetic moment*, rather than *magnetization* (moment per volume), simply because the

raw data from the 2G™ magnetometers are, by the physics of their operating principles, sensitive to the total magnetic moment of a specimen. SQUID magnetometers monitor the differential change in electric current flowing in a pair of Helmholtz-geometry superconducting pick-up rings, and that is directly proportional to the total magnetic flux change across the loops, which is in turn proportional to the magnetic moment of a sample inserted into the center of the sense region (Fuller et al., 1985). The shape of the sample is simply not important (flat discs, cubes, or irregular objects are all OK), as long as the material being measured is brought within the uniform region of the sensor (Kirschvink, 1992). This is different from older methods of measurements such as the astatic, induction-spinning, and fluxgate-ring sensors where the *shape* of individual samples was critically important. Comparing the specimen moment to that of the sample holder is also confusing if one is measured in terms of magnetization, rather than in units of moment.

After initial measurement of the natural remanent magnetizations (NRMs), samples were subjected to two or more low-temperature thermal cycles in liquid nitrogen to help remove any viscous components that might have been carried by multi-domain magnetite. This was followed by a series of low-intensity progressive 3-axis alternating-field (AF) demagnetization experiments evenly spaced up to about 7 mT, again to help remove any soft magnetic components that might have been acquired by exposure to moderate magnetic fields from Airport X-ray machines or during the sample preparation. This was followed by progressive thermal demagnetization under a gentle flow of N_2 gas in a magnetically-shielded oven (<25 nT residual field), starting at 75 °C and incrementing in steps ranging from 10 to 25 °C, until the magnetization vectors were too weak to measure or the specimens displayed unstable behavior. We have found that heating in the N_2 gas helps reduce the oxidation of ferrimagnetic minerals, reducing the problem of the acquisition of spurious components upon mid-level heating steps. If the first specimen from a core displayed erratic or unstable behavior before isolating or revealing the characteristic component, an additional specimen from the sample was run through a similar demagnetization series. To check for chemical changes during thermal demagnetization, we measured the bulk susceptibility after each demagnetization step for each sample using a Bartington™ MS-2 susceptibility bridge that was built into the sample changing system as described elsewhere (Kirschvink et al., 2008). Between 15 and 30 discrete demagnetization experiments were performed per specimen (average 24), on over 320 specimens, for an overall data set of over 7800 complete measurements of NRM. Principle magnetic components were determined using the techniques of Kirschvink (1980), with the parameter for the Maximum Angular Deviation (MAD) set at 15°. Due to the weak nature of the NRMs, components that were trending toward the origin, or formed 'stable endpoint clusters' before the onset of unstable behavior, were fit by forcing the least-squares line through the origin (anchoring).

4.3. Rock magnetism

As the Kamura limestone possesses an unusually weak, but stable, NRM, we conducted a series of rock magnetic investigations to unravel the nature of the magnetic phases present. At the KAM locality, specimens cut from the 40 block samples in the Kobe University collection from across the G/L boundary were subjected to isothermal remanence (IRM) acquisition experiments to access for the presence of ferromagnetic and antiferromagnetic mineral phases. For a sub-set of these specimens we followed the general procedure of Lowrie (1990) for identifying the magnetic minerals present based on the distinctive coercivity and blocking temperature characteristics of hematite, magnetite, and phyrrhotite, respectively. Hematite has both the highest Néel temperature (670°) and coercivity (>1 T) of these minerals, the Néel temperatures of the pyrrhotite mineral family are at or below ~325 °C with intermediate coercivities between ~0.4 and 1 T (Dekkers, 1989), whereas magnetite has a Néel temperature of 580 °C and coercivities below 0.3 T. The progressive thermal demagnetization characteristics of these components are thus diagnostic of these minerals, and can be separated by giving a set of orthogonal isothermal remanent magnetizations (IRMs) of progressively lower value (Lowrie, 1990). We therefore conducted thermal demagnetization of orthogonal IRMs given sequentially at 2.7 T, 400 mT, and 120 mT, at progressively higher peak temperatures up to 680 °C.

To further characterize the NRM, a series of specimens from the same section (8) were subjected to the suite of non-destructive rock magnetic experiments described by Kirschvink et al. (2008) at Caltech, starting with the 3-axis Alternating-field (AF) progressive demagnetization of the NRM in peak fields up to 80 mT. This was then followed by the anhysteretic remanent magnetization (ARM) version of the Lowrie–Fuller test for single-domain behavior (Johnson et al., 1975), which involved progressive acquisition of an ARM in peak alternating-fields (AF) of 100 mT, with variable DC biasing fields of 0–1 mT, followed by progressive AF demagnetization of the maximum ARM. In this test, the ARM substitutes for a weak-field TRM for single-domain and pseudo-single-domain particles, and provides a simple method for evaluating the relative contribution of these to the less geologically stable multi-domain fraction. Samples were then given an IRM pulse in a peak field of 100 mT, followed by progressive AF demagnetization experiments (providing the ARM Lowrie-fuller tests for the fraction of the NRM with coercivities below 100 mT, e.g., (Johnson et al., 1975)). Finally, the samples were subjected to progressive IRM acquisition experiments up to 350 mT, again followed by progressive AF demagnetization.

4.4. Clumped isotopes

Carbonate clumped isotope thermometry (Δ_{47}) is based on the temperature-dependent preference of rare isotopes ^{13}C and ^{18}O to bond with each other within a carbonate lattice. Due to the stronger chemical bond energy, the fraction of CO_2 molecules that contain both ^{13}C and ^{18}O atoms *decreases* as the temperature of crystallization *increases*; recently-developed techniques and calibration allow this 'clumpiness' to be measured easily. This thermometry allows determining independently the temperature at which carbonate crystallized and the $\delta^{18}O$ of the mineralizing fluid (e.g., (Ghosh et al., 2006)), and has mostly been used for paleoclimatological reconstructions (e.g., (Eiler, 2011; Ghosh et al., 2006) and references therein). However, when carbonates experience high temperatures from burial or contact metamorphism, solid-state diffusion of C and O within the mineral lattice might occur, leading to some reordering of ^{13}C–^{18}O bonds on both the prograde and retrograde paths during a geological heating event (Bonifacie et al., 2011; Passey and Henkes, 2012). This has been proposed based on studies of metamorphic marbles that generally show apparent equilibrium temperatures of about ~190 °C (with Δ_{47} averaging 0.352‰; (Bonifacie et al., 2011; Ghosh et al., 2006)) despite peak metamorphic temperatures far above 500 °C. This apparent temperature for marble is thought to represent the "blocking" temperature with respect to diffusional resetting of the carbonate clumped isotope thermometer — that is the temperature at which the isotopes stop exchanging by solid-state diffusion during gradual cooling (Bonifacie et al., 2011; Ghosh et al., 2006). In deeply buried carbonates this phenomenon could therefore potentially challenge, under some circumstances, the reconstruction for both the original temperature of crystallization and the $\delta^{18}O$ value of the mineralizing fluid (because the original distribution of ^{13}C–^{18}O bonds could be progressively lost over heating while the oxygen isotopic composition of the carbonate could still be unaffected if dissolution/recrystallization did not happen), but it could also provide a way to reconstruct burial/heating path conditions (e.g. Bonifacie et al., 2011; Eiler, 2011; Passey and Henkes, 2012).

For this work, CO_2 was released from four samples of limestone, three from the Capitanian Iwato Fm (KAM7-7-2 Shell, KAM7-7-2

Table 1
Clumped isotope results from samples of the Kamura Limestone
Caption = Δ_{47} are reported in ‰ relative to the Ghosh scale, that is compared to a stochastic distribution of ^{13}C–^{18}O bonds in CO_2 that have been heated to 1000 °C (Ghosh et al. (2006)). External precisions on replicate measurements of the same powder are typically ±0.11‰ for both $\delta^{18}O$ and $\delta^{13}C$ and 0.015‰ on Δ_{47} measurements (representing here on average ± 13–20 °C on temperature estimates when one consider the current uncertainties on the equation relating Δ_{47} to temperatures for high temperature materials).

Sample ID	n	$\delta^{13}C$ (‰, PDB)	$\delta^{18}O$ (‰, PDB)	Δ_{47} (‰, Ghosh scale)	Temperature (°C)
KAM7-7-2 Shell	2	4.52	−10.57	0.388	140
KAM7-7-2 Mtx	3	3.79	−10.02	0.414	120
KAM124.2	2	3.35	−7.87	0.406	125
KAM38.2	3	5.60	−9.73	0.391	138
Standard Carrara Marble	10	2.30	−1.72	0.350	190

Matrix, and KAM38.2 in Table 1) and one from the Wuchiapingian Mitai Fm (KAM124.2), using analytical procedures as well as standardization and normalization procedures similar to Ghosh et al. (2006) (i.e., based on CO_2 gases equilibrated at 1000 °C and one carbonate marble reference material). Purified CO_2 was then analyzed at Caltech for its stable isotopic compositions ($\delta^{18}O$, $\delta^{13}C$ and Δ_{47}) on a Finnigan MAT 253 gas source mass spectrometer, configured to collect masses 44 through 49. Measured values of Δ_{47} (reported in ‰ compared to a stochastic distribution of ^{13}C–^{18}O bonds in CO_2 that have been heated at 1000 °C, defined in Ghosh et al. (2006)) were used to estimate carbonate apparent temperatures, using the empirically derived polynomial determined using high temperature experimental calcites (Guo et al., 2009), hydrothermal dolomite (Bonifacie et al., 2011) and inorganic synthetic calcites (Ghosh et al., 2006) all generated into the same intra laboratory frame than the samples investigated here. All samples were analyzed at least twice using sub-fractions of the same powder, to account for heterogeneity.

5. Results

5.1. Composite IRM analysis (Kobe University)

IRM acquisition and thermal demagnetization of composite-IRM experiments shown in supplemental Figs. S1–S5 revealed that magnetite exists ubiquitously through the whole sampled section in concentrations that are almost constant in both the Iwato and the Mitai Formations, except for around the G/L boundary interval. Hematite, however, only exists in the Iwato Formation as the predominant mineral (in terms of bulk volume).

The rock magnetic transition between the Iwato and the Mitai Formations does not match the lithologic boundary, as this change is located a few meters below it. The high proportion of hematite to other magnetic minerals in the Iwato Formation is correlated positively with the Kamura carbon isotope excursion in the same section. Diagenetic processes such as consumption of hematite in the Mitai Formation or formation of hematite in the Iwato Formation are unlikely to explain the predominance of hematite in the Iwato Formation because of the presence of a constant amount of magnetite in both of the Iwato and Mitai Formations. An interpretation of transport from terrestrial origin of hematite is also discarded because of lithologic features of these formations that argue for deposition in an isolated island atoll carbonate platform. Consequently, the rock magnetic properties of the Iwato and the Mitai Formations are most likely depositional features, and the presence of hematite associated with the positive rise in stable carbon isotope ratios probably reflects a change in the paleoenvironment in the superocean Panthalassa, consistent with a rise in environmental oxygen associated with increased carbon burial.

5.2. Coercivity spectral analysis (Caltech RAPID system)

Results from the coercivity analysis generally support the conclusion from the composite IRM analysis, as shown in Fig. 4. The IRM/ARM coercivity spectral analysis of Cisowski (1981) (top row of Fig. 4) shows a broad variability in the Iwato formation, with medium destructive field values spreading between 40 and 60 mT, but with some samples (e.g., KAM 9 and 13) barely starting to approach saturation at peak pulse fields of up to 300 mT, indicating the presence of a high-coercivity antiferromagnetic phase like hematite. All samples from the Mitai formation, however, have much more reproducible coercivity spectra, with medium destructive fields in the 30–40 mT range, and clear approach to saturation by 300 mT suggesting a much smaller antiferromagnetic component. The two formations also differ considerably in their interparticle interaction characteristics as determined by ARM acquisition in the coercivity band <100 mT (second row of Fig. 4). Data from the Iwato formation plot halfway between the chiton tooth and magnetotactic bacterial reference curves, indicating the presence of a mixture of interacting and non-interacting particles. In contrast, the Mitai samples follow a trajectory indicating significantly less interparticle interaction, much more like that of partially collapsed bacterial magnetosomes, as calibrated by Kobayashi et al. (2006). Magnetic particles in both formations are dominated by single-domain (SD) or pseudo-single-domain states as indicated by the ARM version of the Lowrie–Fuller test (Johnson et al., 1975) as shown in the 3rd row in Fig. 4. On all samples, the curve for the progressive AF demagnetization of the ARM lies on top of that for the AF of the IRM, indicating domination by SD particles. However, the interparticle interaction effects (given by the relative separation between the two curves) are clearly stronger for the Iwato formation than for the Mitai, suggesting that something has acted to permit more magnetic clumping.

Fuller et al.'s (1988) test of NRM origin (bottom row in Fig. 4), which compares the intensity of the NRM remaining during AF demagnetization with that of the IRM, strongly supports the interpretation that the NRM signal is a depositional or post-depositional remanent magnetization (DRM or pDRM), rather than a CRM or TRM. This is because the values are nearly 3 orders of magnitude less than the corresponding IRM levels, and nearly 2 orders below the ARM values.

A scan using the Caltech ultra-high resolution SQUID magnetic microscope (Weiss et al., 2001) on a polished surface of a sample from the upper portion of the Iwato Formation (KAM-109, Fig. S6) reveals that the magnetization is diffusely located through the material, rather than being localized in discrete clumps or sedimentary grains.

5.3. Clumped isotopes

Table 1 shows results from the four samples measured for this study. Measured carbon isotope values ($\delta^{13}C_{carb}$) for limestone samples from the Kamura event in Kyushu (Isozaki et al., 2007a) are typically in the range of +3 to as high as +6‰, and oxygen ($\delta^{18}O_{carb}$) is in the range from −11 to −8‰; the values obtained here are in reasonably good agreement. Furthermore, Δ_{47} values of the four investigated samples are remarkably similar (average of 0.400‰ ± 0.012‰ standard deviation) within uncertainties on replicate Δ_{47} measurements (typically ±0.015‰ with respect to standards). When converted into temperature estimates, these results converge toward apparent metamorphic temperature of ~130 °C, suggesting that the actual peak temperature was probably close to this. On the other hand, it is worth noting that at elevated temperatures and particularly where apparent Δ_{47} values approach those seen in marbles, it is very difficult to easily rule out the potential contribution of solid-state diffusion that might have only partly reset bond distribution over a heating path (that would give a lower apparent equilibrium temperature estimated based on Δ_{47} measurement than the actual peak temperature) resulting for instance from tectonics (arc timescale regional heating) or from plutonic/dike intrusion heating. However, our measured Δ_{47} values of Kamura

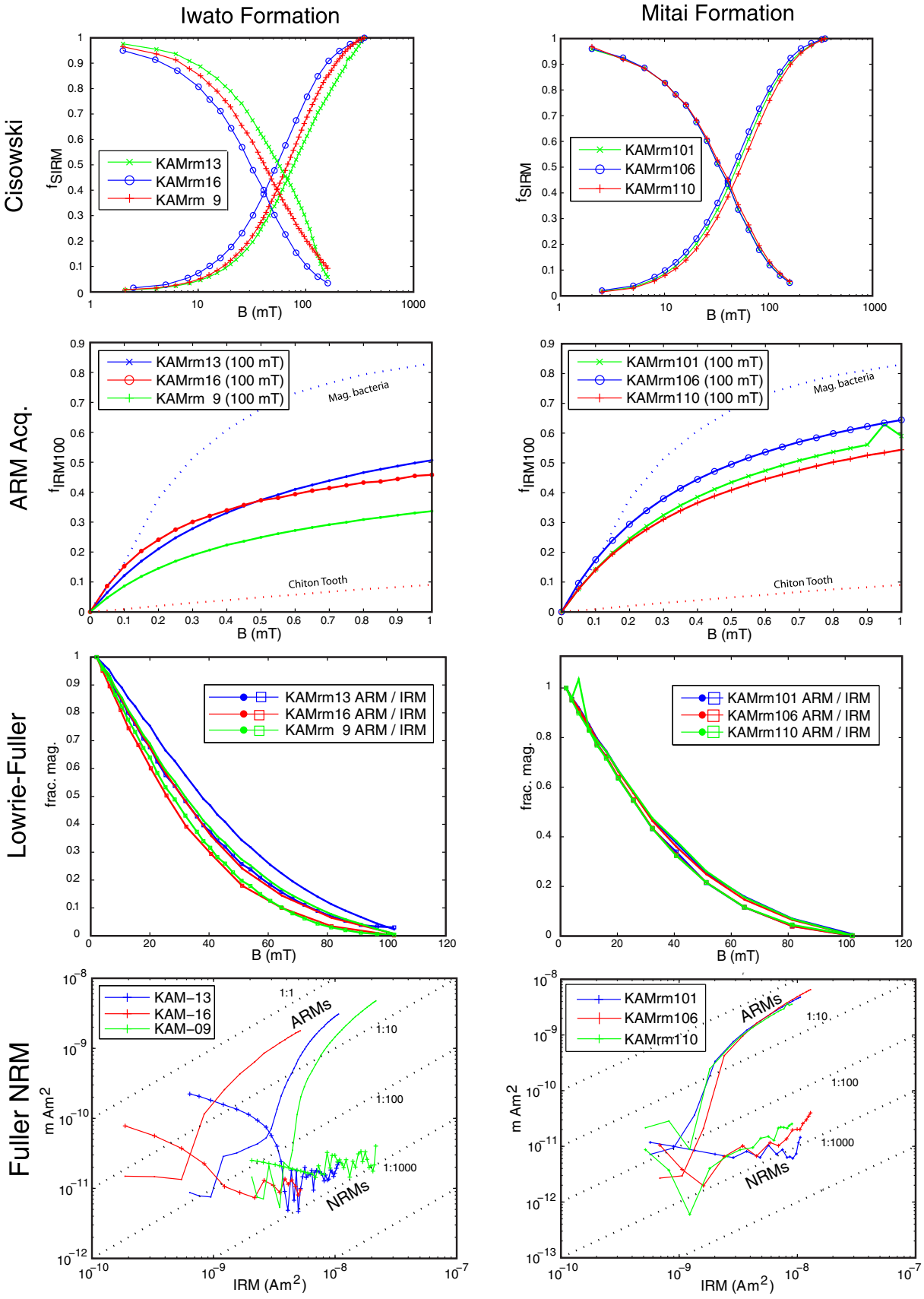

Fig. 4. Rock magnetic results from the Iwato and Mitai Formations, as described in the text. All results are consistent with fine-grained, presumably biogenic magnetite holding the characteristic remanent magnetization.

limestones are significantly higher than the minimum Δ_{47} value of 0.350‰ observed in slowly cooled calcite marbles [corresponding to the apparent equilibrium temperature or "blocking temperature" of 190 °C for the Carrara marble standard, shown for comparison in Table 1]. This suggests that Kamura limestones probably never experienced temperatures higher than 190 °C for a long period of time (i.e., longer than about 10–20 Myr based on parameters defined in Passey and Henkes (2012)), because otherwise they would show Δ_{47} values comparable to Cararra marble. As noted in part 2.3 above, petrographic studies of the large *Alatoconchidae* bivalves show that their external layer retains an arguably primary prismatic calcite, with the original biological alignment of the c-axis perpendicular to the shell surface. Similar petrographic studies of the well-preserved micrites from the Kamura limestone argue that a reasonable fraction of the carbonate has not undergone obvious recrystallization. Higher temperatures ought to have led to petrographic textures and recrystallization typical of marbles, which these rocks do not show. Finally, although some caution is warranted as knowledge on clumped isotopes in high temperature systems is still relatively recent, the most straightforward interpretation of our Δ_{47} results that are consistent to the known geological setting, is that the actual peak heating temperature was close to 130 °C.

5.4. Paleomagnetic results

Specimen-level progressive demagnetization data for six samples from three sections through the Kamura limestone are shown in Figs. S7A–F. The first thing to notice is the unusually weak nature of the NRM, with specimen magnetic moments starting in the range of ~10 to 100 pAm^2 (~10^{-8} to 10^{-7} emu, or about 2 to 20 μA/m for the 5 cm^3 size of our typical specimen; remember that 1 G = 1 emu/cm^3 = 10^{+3} A/m). This is below holder noise on most of the superconducting magnetometer systems in use, and a major reason that previous paleomagnetic studies of rocks with similar lithologies have failed (Ripperdan, 1990; Yokoyama et al., 2007). Putting this in perspective, they are 2 to 3 orders of magnitude weaker than the classic pelagic limestones of Italy, which have NRM magnetizations of ~1 mA/m (Alvarez and Lowrie, 1984). Nevertheless, the data are straightforward to interpret. Low-temperature cycling in liquid nitrogen (steps LT1 and LT2) removes up to ~10% of the NRM intensity, suggesting the presence of occasional grains of MD or SPD magnetite that are unlocked while cycling through the Verway transition (Dunlop and Ozdemir, 1997); these particles could be a remnant of background cosmic dust or volcanic ash in the environment that might be expected to fall into the sediment of a carbonate platform atoll. Directions for the component removed during this low-temperature cycling do not have an obvious grouping, and were presumably gained randomly during sample transport or specimen preparation. Following this, about half of the specimens display a low-coercivity, low blocking temperature overprint with directions similar to the Recent magnetic field direction, which is removed by weak AF demagnetization (up to 7 mT), and/or relatively low thermal treatment (often to only 75 °C). Presumably, this is a combination of viscous remanence, coupled with the presence of trace amounts of goethite formed during surface weathering (which generally carries a Recent or present field direction (PLF) which disappears as the mineral alters at low-temperature treatment). Most specimens at this point either retain or progressively move toward more characteristic remanence (ChRM) directions in two shallow inclination, antipodal groups, in the NNW and SSE directions. The increased scatter in the measurements is a result of the weak intensity of the NRM compared to the combined background noise of the magnetometer and sample holders.

One problem that arises commonly in paleomagnetic studies concerns the recognition and separation of such soft (PLF) components from earlier, characteristic (ChRM) directions. It helps if post-depositional tilting of the units (and/or polar wander) creates a clear angular separation between the components, although at best the two directions can be orthogonal. The limestone block in the accretionary complex of the Kamura region is tilted so that the bedding is now nearly vertical, but the axis of the mean PLF component removed by the initial low demagnetization treatment only has an angular separation of about 16° from the nearest axis of the ChRM direction (that to the NNW; see below). This case is therefore similar to that of younger, flat-lying rocks where the distribution of the two components also overlaps. We have therefore followed the Principal Component procedure described by Tobin et al. (2012), in which we first examine data from samples that have the ChRM direction furthest from the PLF direction, to gain an understanding of their relative stability spectra. We assume that the overprint is not influenced by the direction of the underlying ChRM direction, and therefore use that as a guide for separating them during the Principal Component Analysis. As noted by Tobin et al., the scatter of the secular variation is often large enough so that clear 'kinks' appear in the vector demagnetization diagrams that allow separation of the components. This is discussed in more detail in Fig. S7.

Results of the Principal Component Analysis (PCA) on the demagnetization data from the Kamura limestone are shown in Fig. 5 and Table 2. The soft component clusters around the expected direction for the Recent geomagnetic field, as indicated in Fig. 5A, and is identified as PLF in Table 2. In contrast, those specimens that contain a component of higher stability, the 'Characteristic Remanence' or ChRM, fall into two distinct clusters. After correction for the local tilt of bedding these lie to the NNW with generally shallow upward directions, and the opposite group is to the SSE with shallow down inclination (Fig. 5B). We emphasize that this ChRM direction is relatively weak compared to normal paleomagnetic studies. Using the matrix deconvolution method of Jones (2002), we have been able to estimate the total magnetic moment of the ChRM vector in some of our samples from the KAM locality (Section 8 in Fig. 2), and plot them in Fig. 5C as a function of the geometric grouping parameter for linearity (MAD value, e.g., (Kirschvink, 1980)). Stable directions are recoverable down to intensities of less than 10 pAm^2 (10^{-8} emu). In a similar fashion, the ChRM component data can be analyzed to yield an idea of the range of blocking temperatures that hold it by making a survivorship curve showing the last temperature step that provides a useable point for the PCA analysis. As shown in Fig. 5D, these thermal termination points are distributed between ~200° and 400 °C, with about 1/3 of the loss happening between 375° and 400 °C. Although well below the Néel temperatures of the two major magnetic minerals present (magnetite and hematite, see Section 5.1 above), blocking temperatures are particle-size dependent and often fall in this range in natural samples (such as bacterial magnetofossils.) This stability range is also compatible with the preservation of a primary remanence for fine-grained magnetite on geological time scales (Pullaiah et al., 1975).

Table 2 shows summary statistics of the PLF and ChRM components, the latter being given in coordinates of both in-situ and after correction for the local tilt of bedding, following the combined line and plane analysis of McFadden and McElhinny (1988). Directions are also presented separating out samples according to polarity, as well as a grouping in which only data from specimens that yielded the least-squares lines are analyzed. Table S1 shows results of directional statistics tests. Watson's (1956) test of common Fisher's precision parameter (κ) indicates that the distributions are similar in both the NOR and REV cases, with or without the inclusion of demagnetization arcs, and that the κ value for the PLF component is also similar to those for the ChRM. In either grouping (all data, or only demagnetization lines), the ChRM data show a positive "Category B" reversals test, using the classification of McFadden & McEllhinny (McFadden and McElhinny, 1990). In particular, the angular separation of the two antipolar groups using all of the data is only 1.0°, whereas the critical angle for 95% confidence is 6.5°. Similarly, the axis of the PLF component, which lies 16.0° from the ChRM axis, is statistically distinct from this at an extraordinarily high confidence level. These data imply that the Kamura Limestone Atoll formed at a paleolatitude of ~12°, and the pole position is far from any other reported direction from the South China Block (e.g., (Wang et al., 1993; Yang and Besse, 2001)).

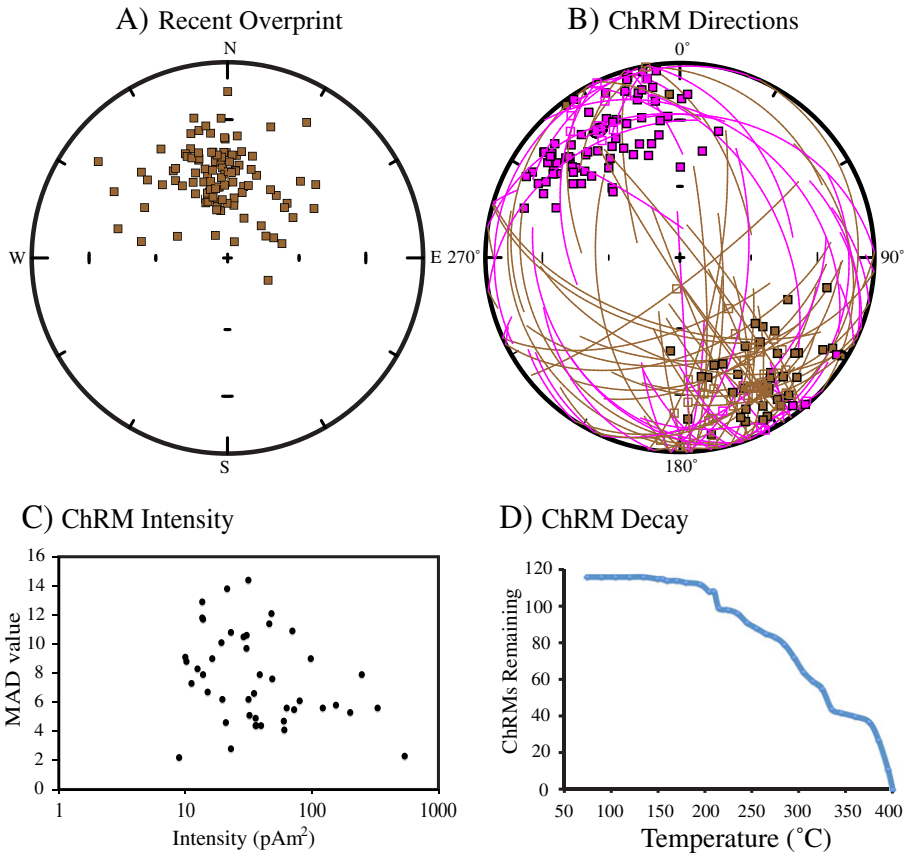

Fig. 5. Results of the Principal Component Analysis. A. Low-coercivity and low-T components interpreted to be of Recent origin (PLF component, in-situ.). B. Two-polarity characteristic direction, NOR and REV, tilt-corrected coordinates. Arc-constraints for samples that do not reach the stable endpoints are calculated with the method of McFadden and McElhinny (1988), and are shown with the open symbols on the arc traces. Pink symbols indicate upper hemisphere directions. C. A summary of the maximum angular deviation from the principal component analysis plotted against intensity of the fit principal component directions using the matrix deconvolution (J/Jo routine) of Jones (2002), described further in Kirschvink et al. (2008). D. Survivorship curve, showing the maximum temperature recorded for the ChRM component in each specimen as a function of temperature.

5.5. Magnetostratigraphy

Fig. 6 shows a summary comparison of the magnetic polarity results for the Kamura limestones, as documented further in Supplemental Figs. S7–9, and in the archived paleomagnetic data summary (MagIC data acquisition # XXXXX). The stratigraphically oldest interval, exposed in Section 2 (Saraito) starts in the *N. craticulifera* Zone (lower Wordian), and has a prominent switch in magnetic polarity between

Table 2
Paleomagnetic results from Upper Permian Limestones from Kyushu reported in this study.
L = lines; P = planes; N = number of samples; Dec. = declination; Inc. = inclination; κ = Fisher's precision parameter; α9 = 95% confidence cone; VGP lat. = virtual geomagnetic pole latitude; VGP lon. = VGP longitude. *Values in these rows have been corrected for the tilt of bedding.
The field area in Kyushu, Japan is located approximately at 32.8° N, 131.3° E.

Components:	N	Dec.	Inc.	κ	R	α95
PLF	105	354.1	55.5	15.20	98.2	3.7
ChRMs						
Normal lines	76	319.4	69.1	11.12	69.3	5.1
*		*327.0*	*−24.4*	*12.86*	*70.2*	*4.7*
Reversed lines	43	152.8	−62.5	15.12	40.2	5.8
*		*144.0*	*22.7*	*14.83*	*40.2*	*5.9*
Normal L + arcs	84	321.4	69.5	11.48	76.8	4.8
*		*327.9*	*−23.6*	*13.27*	*77.7*	*4.4*
Reversed L + arcs	65.5	158.3	−61.7	14.89	61.2	4.7
*		*147.0*	*23.1*	*14.81*	*61.1*	*4.7*
All (N + R) lines	119	145.1	−66.8	12.03	109.2	3.9
*		*325.9*	*−23.8*	*13.56*	*110.3*	*3.7*
Best estimate of ChRM:						
(N + R) lines & arcs	149.5	149.6	−66.6	12.33	137.5	3.4
*		*327.5*	*−23.4*	*13.99*	*138.9*	*3.2*
Pole position:						
Pole latitude:	35.3°	A95:	2.5°			
Pole longitude:	351.4°	dp, dm:	1.8°,3.5°			
		Paleolatitude:	−12.2 ± 1.8°			

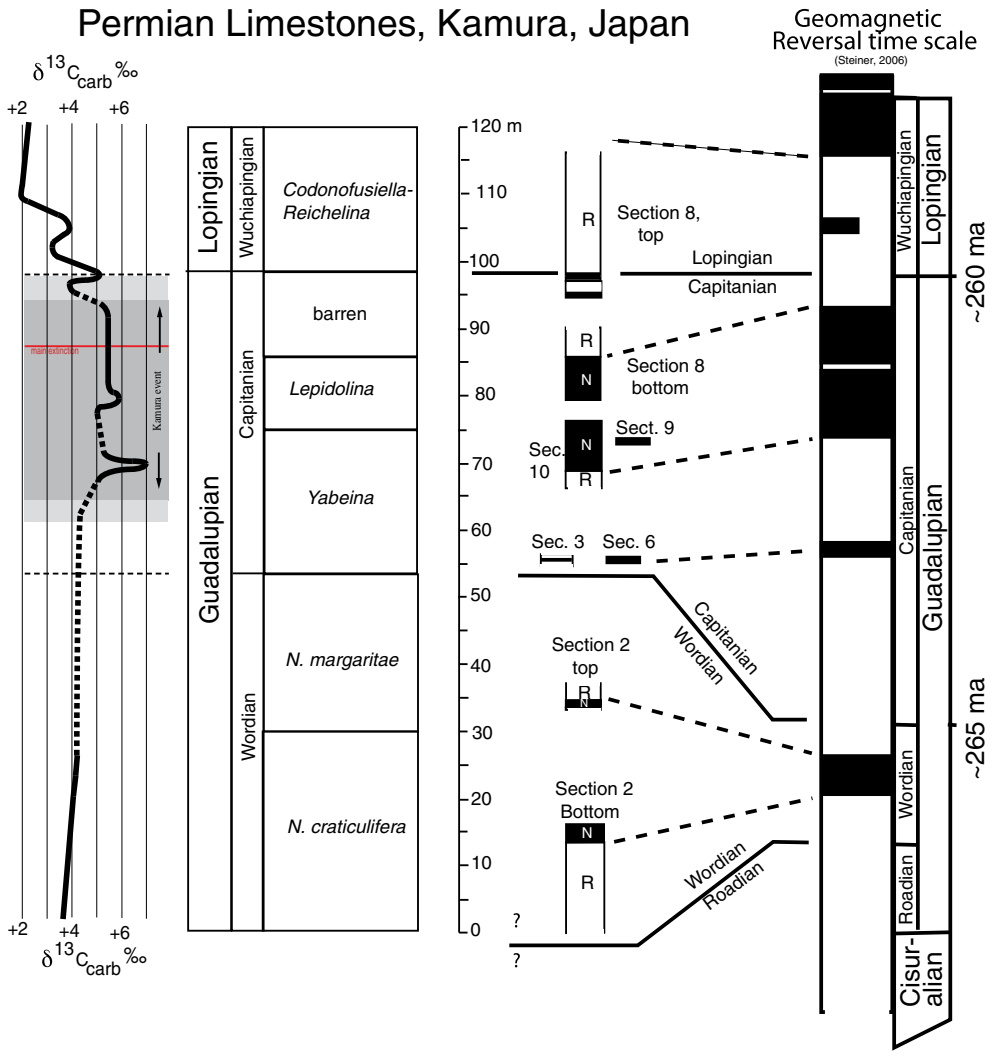

Fig. 6. Magnetostratigraphy of the Permian Limestones of Kamura, Kyushu, Japan, compared with biostratigraphic and carbon isotope constraints. Data for the major sections are in the supplemental information, Figs. S8–10. Note that the summary ignores occasional one-point samples with opposite polarity. Data for the Kamura carbon isotope anomaly are from (Isozaki, 1997a,b).

~10 and 12 m in the section. This is approximately the position inferred for the top of the Permian Long Reversed Chron, known as the "Illawara" reversal at the top of the Kiaman Reversed Interval (e.g., (Steiner, 2006)). This implies that the North-Westerly and shallow-up polarity of the ChRM directions are of Normal polarity, and the South-Easterly and shallow down directions are Reversed.

Using this polarity interpretation, the Wordian (*N. craticulifera* and *N. margaritae* Zones) sampled at Section 2 (Fig. S9) is characterized by a clear reversed interval in the bottom 11 m of section, followed by an interval where 7 of the next 10 samples appear to be of normal polarity (unfortunately separated by a 15 m thick covered interval). The Capitanian *Yabeina* and *Lepidolina* zones are characterized by solid normal interval that is easily correlated with that reported from the Capitanian from the rest of the world (Gradstein et al., 2012; Steiner, 2006). On the other hand, the barren interval of the topmost Capitanian is dominated by a reverse interval. This interval is possibly correlated with the reverse interval recognized in the upper Capitanian *J. granti* Zone in South China (Shen et al., 2010).

This interpretation is consistent with the remaining portions of the stratigraphy, in which the top of Section 2 lies in the *N. margaritae* Zone (upper Wordian), and should be N/R. Section 10 in the upper *Yabeina* Zone (lower Capitanian) has a R/N transition, with the N extending into the lower Lepidolina Zone. This switches to dominantly R through the basal portion of the 'barren' interval in section 8 (uppermost Capitanian) and extends well into Lopingian time (*Codonofusiella–Reichelina* Zone of the Wuchiapingian). Smaller stratigraphic intervals of Sections 2, 3, 6, and 9 are consistent with this interpretation, as shown in Fig. 6.

This polarity interpretation constrains the paleolatitude of the Permian Iwato and Mitai Limestone at Kamura to be at $-12.2 \pm 1.8°$ *South*, as indicated in Table 2.

6. Discussion

6.1. Stability and origin of the NRM

Although they possess an unusually weak magnetization, several lines of evidence support the hypothesis that samples of the late Permian limestone from the Kamura area possess a primary remanent magnetization. Unrecrystallized calcite in the molluscan shell nacre and the clumped isotope results are most consistent with peak temperatures below ~130 °C. In addition, the positive reversals test on the ChRM component, its thermal stability spectrum, and the generally good agreement of the reversal stratigraphy with other late Permian results argue for a primary, or early diagenetic origin of this component, most likely held in fine-grained magnetite. Coupled with the excellent biostratrigraphic and chemostratigraphic constraints on the sequence, the paleomagnetic pole position calculated from this sequence scores

a perfect 7/7 on the Vandervoo (Vandervoo, 1990) scale of paleomagnetic reliability.

Other than a light scattering of cosmogenic or volcanic dust, most of the magnetization appears to be held in moderately interacting, very fine-grained, single-domain or pseudo-single-domain magnetite. The most likely origin of this material is production by the magnetotactic bacteria, as they are known to inhabit similar carbonate-rich environments (Chang and Kirschvink, 1989; Chang et al., 1987; Kirschvink and Chang, 1984; Kirschvink and Lowenstam, 1979; Kopp and Kirschvink, 2008; Maloof et al., 2007) and have similar rock magnetic properties, including the inter-grain interaction effects (Kobayashi et al., 2006). They have also been implicated in the magnetization of platform carbonates from younger ocean island atolls (e.g., (Aissaoui and Kirschvink, 1991; Aissaoui et al., 1990)), as well as in a variety of pelagic marine carbonates (Roberts et al., 2013).

An interesting twist on this result is the rock magnetic evidence from the composite IRM experiments (Figs. S1–5) for the presence of a significant fraction of detrital hematite in sediments of the Iwato formation mentioned in Section 5.1 above. This unit preserves significantly less organic matter than the underlying Mitai formation, and the association of the hematite with the positive excursion of $\delta^{13}C_{carb}$ argues for a mechanistic link. We suggest that the spike in $\delta^{13}C_{carb}$ actually reflects an increase in the fraction of volcanic carbon (emitted as CO_2) being buried as organic carbon, with an implied 1–1 rise in atmospheric oxygen concentration. For shallow-water carbonates, an increased oxygen level would account for the more oxidized character of these sediments

6.2. Middle–Upper Permian magnetostratigraphy and bio- and chemostratigraphic correlation

Our data reveal multiple geomagnetic polarity changes within the Guadalupian Iwato Formation primarily from low-latitude mid-Panthalassa. As summarized in Fig. 6, the lower half (Wordian part) of the Iwato Formation is dominated by reversely magnetized intervals, whereas the upper half (Capitanian part) by normal ones. In contrast, the lower part of the overlying Mitai Formation above the G–LB recorded a stable reversed interval. This overall aspect is in general agreement with previous compilations of Permian magnetostratigraphy (e.g., (Gradstein et al., 2012; Steiner, 2006)).

It is particularly noteworthy that a short normal interval appears around the G–LB (Fig. 6). This signal is possibly correlated with the magnetostratigraphic record from South China that is characterized by a short-term normal interval for the *Clarkina postbitteri honshuiensis* Zone that defines the topmost Capitanian at the GSSP of G–LB in South China (Shen et al., 2010). This correlation is supported by the stable carbon isotope stratigraphy, because a sharp negative shift for ca. 3‰ (from +5 to +2‰) was reported from the upper part of the barren interval (Isozaki et al., 2007b). This shift is chemostratigraphically correlated with the same signature in the *C. postbitteri honshuiensis* Zone and *C. postbitteri postbitteri* Zone across the G–LB at the GSSP in Penglaitan (Chen et al., 2011; Wang et al., 2004).

Similarly, the consistently reversely magnetized interval in the lowermost *Codonofusiella–Reichelina* Zone of the Mitai Formation also fits into the reverse interval reported from the topmost *C. postbitteri honshuiensis* Zone, *C. postbitteri postbitteri* Zone, and the lowermost *C. dukoensis* Zone across the G–LB at the GSSP in South China (Shen et al., 2010).

These data add validity not only to the biostratigraphic correlation based on fusuline zones in the paleo-atoll sections in Japan (Ota and Isozaki, 2006) and conodont zones in shelf sequences in South China (Shen and Mei, 2010), but also to the chemostratigraphical correlation based on stable carbon isotope ratio of carbonates (Isozaki, 1997a,b). The *Yabeina* and *Lepidolina* zones of the Iwato Formation are correlated with the Capitanian conodont zones; i.e. the *Jinogondolella postserrata* Zone to *J. granti* Zone, whereas the barren interval of the uppermost Iwato Formation likely corresponds to the *C. postbitteri honshuiensis* Zone that marks the uppermost Capitanian conodont zone, in South China.

6.3. Identifying the Illarawa Reversal

From the viewpoint of magnetostratigraphy, it is particularly noteworthy that the lower part of the Iwato Formation is characterized by the presence of samples with clear normal polarity in the *N. craticulifera* Zone of early Wordian age, which continues up into the overlying *N. margaritae* Zone of late Wordian age. These data indicate that a normal interval surely appeared in the Wordian, probably for the first time since the Late Carboniferous. A long-lasting "reverse interval" that continued for ca. 50 million years from the Late Carboniferous to the Middle Permian has been widely known as the Kiaman Reverse Superchron (Irving and Parry, 1963). The 'Illawarra Reversal' is an informal term used to mark the top of the Kiaman Reverse Superchron, or the base of the Permian–Triassic Mixed Superchron (Gradstein et al., 2012; Irving and Parry, 1963; Isozaki, 2009; Steiner, 2006). Nonetheless, its age has not been precisely determined because it was originally detected in the non-marine coal measures in eastern Australia that lack diagnostic marine index fossils for global correlation. Therefore, previous summaries for the Permian magnetostratigraphy were not necessarily consistent from each other, particularly for the Wordian interval. For example, Ogg et al. (2008) placed the Illawarra Reversal at the base of the Capitanian, whereas Steiner (2006) and Henderson et al. (2012) put it in the middle of the Wordian. Unfortunately, there are numerous problems in compiling the late Permian information, as much of the data discussed by Steiner (2006) are unpublished, and many of the sections in Europe and Africa are in continental facies, where the correlations to the marine realm are uncertain(Szurlies, 2013; Ward et al., 2005). Our data clearly show Normal chrons both in mid-Wordian time and mid to late Capitanian time, with good biostratigraphic and chemostratigraphic constraints (Ota and Isozaki, 2006).

The present data confirm that the Capitanian part (the *Yabeina* Zone and *Lepidolina* Zone) possesses normal intervals. As to possible normal sub-chrons in the Wordian, however, two interpretations are possible: 1) these signals can be regarded as small-scale geomagnetic noise within the Kiaman Reverse Superchron, and the Illawarra Reversal in mid-superocean is stratigraphically placed around the G–LB as Ogg et al. (2008) proposed, or 2) one of them represents the first appearance of a solid normal interval that pins down the Illawarra Reversal in mid-Wordian time. Judging from the frequent appearance of normal signals, we prefer the latter interpretation here, in accordance with the compilations of Steiner (2006) and Henderson et al. (2012).

6.4. Migration history of seamount and paleobiogeographical implications

The present paleomagnetic data demonstrate a long travel distance of the Permian mid-superoceanic seamount capped by a paleo-atoll complex. Around the G–L boundary, ~260 Ma, the seamount was accumulating shallow marine atoll carbonates at 12.2 ± 1.8° S in the middle of the Panthalassic ocean. The seamount later migrated toward northwest to eventually accrete to the Japan (= South China) margin at mid-latitude in the northern hemisphere during the mid-Jurassic (ca. 165–160 Ma), as indicated schematically in Fig. 7. The paleomagnetic data (and polarity interpretation) imply that it was subjected to a vertical-axis rotation (w.r.t. North) of only about 30° CCW, over its entire history. The total travel distance of the seamount within western Panthalassa likely reached ~3000 km, assuming a typical plate convergence rate of 3 cm/year, and 100 myr to dock. During the northward migration of the seamount, it likely crossed a paleo-biogeographic provincial boundary, i.e. a border between the two contemporary fusuline territories (e.g., Kasuya et al. (2012)). In fact, Kasuya et al. (2012) were the first to document the practical location of a mid-oceanic biogeographic province boundary within the pre-Jurassic lost oceans. We emphasize here that similar paleomagnetic studies on weakly

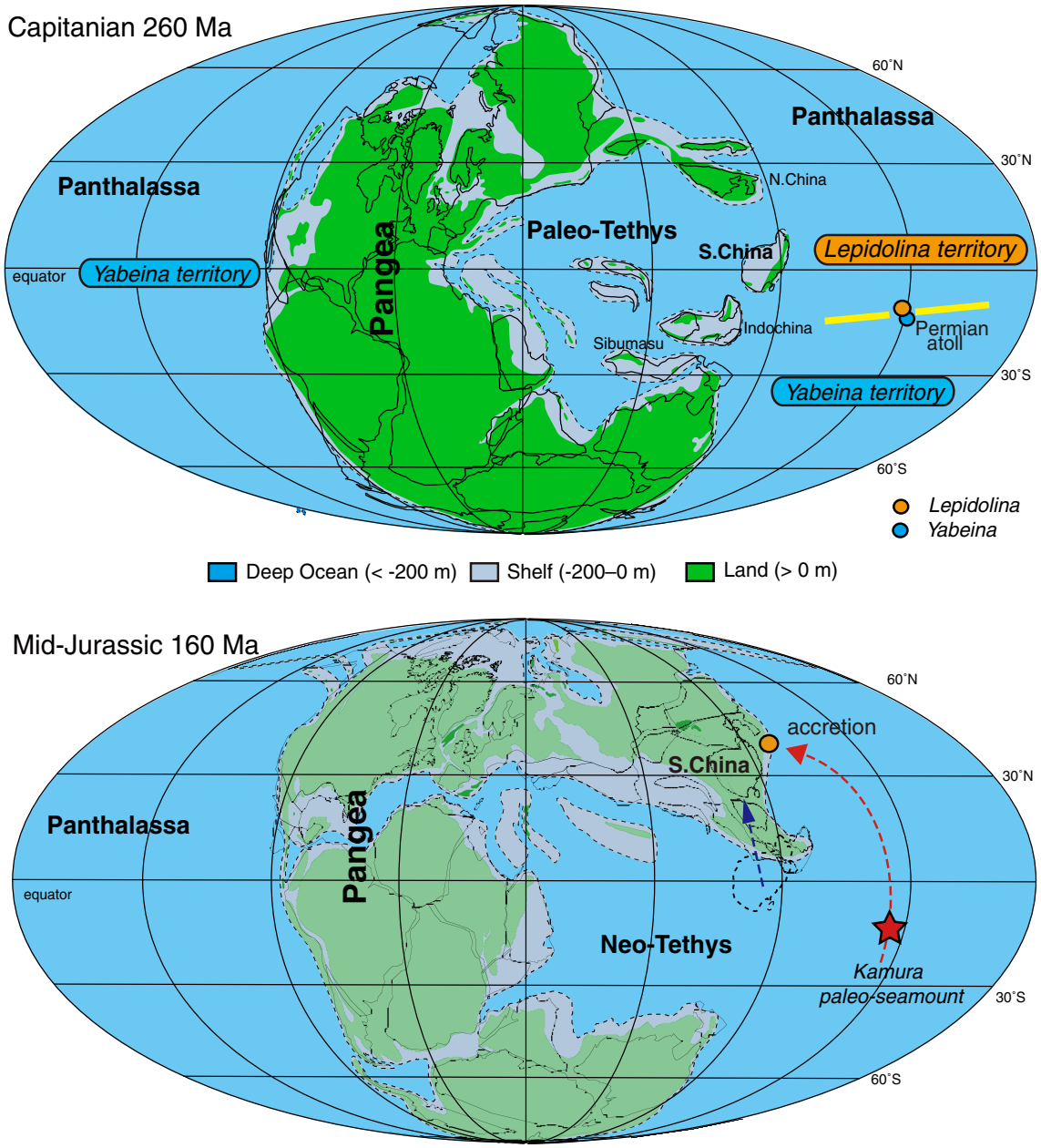

Fig. 7. Paleogeographic maps showing location of the Kamura seamount in late Permian and Jurassic time. Adapted from Kasuya et al. (2012).

magnetized paleo-atoll carbonates on migrating seamounts should have many further applications in paleobiogeography, in particular for the lost wide oceanic domains in the past.

Acknowledgments

We thank Tomomi Kani of Kumamoto University, Masafumi Saitoh, Tomohiko Sato, and Daisuke Kofukuda of the University of Tokyo (Komaba) for their help in field work, and John Eiler of the California Institute of Technology for use of mass spectrometer for clumped isotope measurements.

Appendix A. Supplementary data

Supplementary data to this article can be found online at http://dx.doi.org/10.1016/j.palaeo.2014.10.037.

References

Abrajevitch, A., Kodama, K., 2009. Biochemical vs. detrital mechanism of remanence acquisition in marine carbonates: a lesson from the K–T boundary interval. Earth Planet. Sci. Lett. 286, 269–277.
Abrajevitch, A., Hori, R.S., Kodama, K., 2011. Magnetization carriers and remagnetization of bedded chert. Earth Planet. Sci. Lett. 305, 135–142.
Aissaoui, D.M., Kirschvink, J.L., 1991. Atoll magnetostratigraphy — calibration of the Eustatic records. Terra Nova 3, 35–40.
Aissaoui, D.M., McNeill, D.F., Kirschvink, J.L., 1990. Magnetostratigraphic dating of shallow-water carbonates from Mururoa atoll, French Polynesia: implications for global eustasy. Earth Planet. Sci. Lett. 97, 102–112.
Alvarez, W., Lowrie, W., 1984. Magnetic stratigraphy applied to synsedimentary slumps, turbidites, and basin analysis; the Scaglia Limestone at Furlo (Italy). Geol. Soc. Am. Bull. 95, 324–336.
Alvarez, W., Kent, D.V., Silva, I.P., Schweickert, R.A., Larson, R.A., 1980. Franciscan complex limestone deposited at 17° south paleolatitude. Geol. Soc. Am. Bull. 91, 476–484.
Ando, A., Kodama, K., Kojima, S., 2001. Low-latitude and Southern Hemisphere origin of Anisian (Triassic) bedded chert in the Inuyama area, Mino terrane, central Japan. J. Geophys. Res. Solid Earth 106, 1973–1986.
Bonifacie, M., Ferry, J.M., Horita, J., Vasconcelos, C., Passey, B.H., Eiler, J.M., 2011. Calibration and applications of the dolomite clumped isotope thermometer to high temperatures. Mineral. Mag. 75, 551.

Butler, R.F., 1992. Paleomagnetism: Magnetic Domains to Geologic Terranes. Blackwell Scientific Publications, Boston.
Chang, S.-B.R., Kirschvink, J.L., 1989. Magnetofossils, the magnetization of sediments, and the evolution of magnetite biomineralization. Ann. Rev. Earth Planet. Sci. 17, 169–195.
Chang, S.-B.R., Kirschvink, J.L., Stolz, J.F., 1987. Biogenic magnetite as a primary remanence carrier in limestone. Phys. Earth Planet. Inter. 46, 289–303.
Chen, B., Joachimski, M.M., Sun, Y.D., Shen, S.Z., Lai, X.L., 2011. Carbon and conodont apatite oxygen isotope records of Guadalupian–Lopingian boundary sections: climatic or sea-level signal? Palaeogeogr. Palaeoclimatol. Palaeoecol. 311, 145–153.
Cisowski, S., 1981. Interacting vs. non-interacting single-domain behavior in natural and synthetic samples. Phys. Earth Planet. Inter. 26, 56–62.
Cottrell, R.D., Tarduno, J.A., Roberts, J., 2008. The Kiaman reversed polarity superchron at Kiama: toward a field strength estimate based on single silicate crystals. Phys. Earth Planet. Inter. 169, 49–58.
Courtillot, V., Olson, P., 2007. Mantle plumes link magnetic superchrons to phanerozoic mass depletion events. Earth Planet. Sci. Lett. 260, 495–504.
Dekkers, M.J., 1989. Magnetic-properties of natural pyrrhotite 2. High-temperature and low-temperature behavior of Jrs and TRM as a function of gain-size. Phys. Earth Planet. Inter. 57, 266–283.
Dunlop, D.J., Ozdemir, O., 1997. Rock Magnetism: Fundamentals and Frontiers. Cambridge University Press, New York.
Eiler, J.M., 2011. Paleoclimate reconstruction using carbonate clumped isotope thermometry. Quat. Sci. Rev. 30, 3575–3588.
Epstein, A.G., Epstein, J.L., Harris, L.D., 1977. Conodont color alteration — an index to organic metamorphism. Geol. Soc. Am. Spec. Pap. 153, 108.
Fuller, M., Goree, W.S., Goodman, W.L., 1985. An introduction to the use of SQUID magnetometers in biomagnetism. In: Kirschvink, J.L., Jones, D.S., MacFadden, B.J. (Eds.), Magnetite Biomineralization and Magnetoreception in Organisms: a New Biomagnetism. Plenum Press, New York, pp. 103–151.
Fuller, M., Cisowski, S., Hart, M., Haston, R., Schmidke, E., Jarrard, R., 1988. NRM: IRM(s) demagnetization plots; an aid to the interpretation of natural remanent magnetization. Geophys. Res. Lett. 15, 518–521.
Ghosh, P., Adkins, J., Affek, H., Balta, B., Guo, W.F., Schauble, E.A., Schrag, D., Eiler, J.M., 2006. 13C–18O bonds in carbonate minerals: a new kind of paleothermometer. Geochim. Cosmochim. Acta 70, 1439–1456.
Gialanella, P.R., Heller, F., Haag, M., Nurgaliev, D., Borisov, A., Burov, B., Jasonov, P., Khasanov, D., Ibragimov, S., Zharkov, I., 1997. Late Permian magnetostratigraphy on the eastern Russian platform. Geol. En Mijnbouw 76, 145–154.
Gradstein, F., Ogg, J.G., Schmitz, M., Ogg, G., 2012. The Geological Time Scale 2012. Elsevier, Boston.
Guo, W., Mosenfelder, J.L., Goddard, W.A., Eiler, J.M., 2009. Isotopic fractionations associated with phosphoric acid digestion of carbonate minerals: insights from first principles theoretical modeling and clumped isotope measurements. Geochim. Cosmochim. Acta 73, 7203–7225.
Henderson, C.M., Davydov, V.I., Wardlaw, B.R., 2012. The Permian period. In: Gradstein, F.M., Ogg, J.G., Schmitz, M.D., Ogg, G.M. (Eds.), The Geologic Time Scale 2012. Elsevier, Amsterdam, pp. 653–679.
Irving, E., 1964. Paleomagnetism and its Application to Geologic and Geophysical Problems. Wiley, New York, New York.
Irving, E., Parry, L.G., 1963. The magnetism of some Permian rocks from New-South-Wales. Geophys. J. R. Astron. Soc. 7, 395–411.
Isozaki, Y., 1997a. Contrasting two types of orogen in Permo-Triassic Japan: accretionary versus collisional. Island Arc 6, 2–24.
Isozaki, Y., 1997b. Jurassic accretion tectonics of Japan. Island Arc 6, 25–51.
Isozaki, Y., 2006. Guadalupian (Middle Permian) giant bivalve Alatoconchidae from a mid-Panthalassan paleo-atoll complex in Kyushu, Japan: a unique community associated with Tethyan fusulines and corals. Proc. Jpn. Acad. Ser. B Phys. Biol. Sci. 82, 25–32.
Isozaki, Y., 2009. Illawarra Reversal: the fingerprint of a superplume that triggered Pangean breakup and the end-Guadalupian (Permian) mass extinction. Gondwana Res. 15, 421–432.
Isozaki, Y., 2014. Memories of Pre-Jurassic Lost Oceans: how to retrieve them from extant lands. Geosci. Can. 41, 283–311.
Isozaki, Y., Aljinovic, D., 2009. End-Guadalupian extinction of the Permian gigantic bivalve Alatoconchidae: end of gigantism in tropical seas by cooling. Palaeogeogr. Palaeoclimatol. Palaeoecol. 284, 11–21.
Isozaki, Y., Ota, A., 2001. Middle–Upper Permian (Maokouan-Wuchiapingian) boundary in mid-oceanic paleo-atoll limestone of Kamura and Akasaka, Japan. Proc. Jpn. Acad. Ser. B Phys. Biol. Sci. 77, 104–109.
Isozaki, Y., Maruyama, S., Furuoka, F., 1990. Accreted oceanic materials in Japan. Tectonophysics 181, 179–205.
Isozaki, Y., Kawahata, H., Minoshima, K., 2007a. The Capitanian (Permian) Kamura Cooling Event: the beginning of the Paleozoic–Mesozoic transition. Palaeoworld 16, 16–30.
Isozaki, Y., Kawahata, H., Ota, A., 2007b. A unique carbon isotope record across the Guadalupian–Lopingian (Middle–Upper Permian) boundary in mid-oceanic paleo-atoll carbonates: the high-productivity "Kamura event" and its collapse in Panthalassa. Glob. Planet. Chang. 55, 21–38.
Isozaki, Y., Aljinovic, D., Kawahata, H., 2011. The Guadalupian (Permian) Kamura event in European Tethys. Palaeogeogr. Palaeoclimatol. Palaeoecol. 308, 12–21.
Jin, Y.G., Zhang, J., Shang, Q.H., 1994. Two phases of the end-Permian mass extinction. In: Embry, A.F., Beauchamp, B., Glass, D.J. (Eds.), Pangea: Global Environments and ResourcesMemoir. Canadian Society of Petroleum Geologists, pp. 813–822.
Johnson, H.P., Lowrie, W., Kent, D.V., 1975. Stability of ARM in fine and course grained magnetite and maghemite particles. Geophys. J. R. Astron. Soc. 41, 1–10.
Jones, C.H., 2002. User-driven integrated software lives: "Paleomag" paleomagnetics analysis on the Macintosh. Comput. Geosci. 28, 1145–1151.
Kambe, N., 1963. On the boundary between the Permian and Triassic Systems in Japan with the description of the Permo–Triassic formations at Takachiho-cho, Miyazaki Prefecture in Kyushu and the Skytic fossils contained. Geological Survey of Japan Report, pp. 1–68.
Kani, T., Fukui, M., Isozaki, Y., Nohda, S., 2008. The Paleozoic minimum of Sr-87/Sr-86 ratio in the Capitanian (Permian) mid-oceanic carbonates: a critical turning point in the Late Paleozoic. J. Asian Earth Sci. 32, 22–33.
Kani, T., Hisanabe, C., Isozaki, Y., 2013. The Capitanian (Permian) minimum of Sr-87/Sr-86 ratio in the mid-Panthalassan paleo-atoll carbonates and its demise by the deglaciation and continental doming. Gondwana Res. 24, 212–221.
Kanmera, K., Nakazawa, K., 1973. Permian–Triassic relationships and faunal changes in the eastern Tethys. In: Logan, A., Hills, L.V. (Eds.), The Permian and Triassic Systems and their Mutual Boundary. Canadian Society of Petroleum Geologists Memoir, pp. 100–119.
Kasuya, A., Isozaki, Y., Igo, I., 2012. Constraining paleo-latitude of a biogeographic boundary in mid-Panthalassa: Fusuline province shift on the Late Guadalupian (Permian) migrating seamount. Gondwana Res. 21, 611–623.
Kirschvink, J.L., 1980. The least-squares line and plane and the analysis of paleomagnetic data: examples from Siberia and Morocco. Geophys. J. R. Astron. Soc. 62, 699–718.
Kirschvink, J.L., 1981. How sensitive should a rock magnetometer be for use in paleomagnetism? In: Weinstock, H., Overton, W.C. (Eds.), SQUID Applications to Geophysics. The Society of Exploration Geophysicists, Tulsa, Oklahoma, pp. 111–114.
Kirschvink, J.L., 1992. Uniform magnetic fields and Double-wrapped coil systems: improved techniques for the design of biomagentic experiments. Bioelectromagnetics 13, 401–411.
Kirschvink, J.L., Chang, S.-B.R., 1984. Ultra fine-grained magnetite in deep-sea sediments: possible bacterial magnetofossils. Geology 12, 559–562.
Kirschvink, J.L., Lowenstam, H.A., 1979. Mineralization and magnetization of chiton teeth: paleomagnetic, sedimentologic, and biologic implications of organic magnetite. Earth Planet. Sci. Lett. 44, 193–204.
Kirschvink, J.L., Kopp, R.E., Raub, T.D., Baumgartner, C.T., Holt, J.W., 2008. Rapid, precise, and high-sensitivity acquisition of paleomagnetic and rock-magnetic data: development of a low-noise automatic sample changing system for superconducting rock magnetometers. Geochem. Geophys. Geosyst. 9, 1–18.
Kobayashi, A., Kirschvink, J.L., Nash, C.Z., Kopp, R.E., Sauer, D.A., Bertani, L.E., Voorhout, W.F., Taguchi, T., 2006. Experimental observation of magnetosome chain collapse in magnetotactic bacteria: sedimentological, paleomagnetic, and evolutionary implications. Earth Planet. Sci. Lett. 245, 538–550.
Kodama, K., Takeda, T., 2002. Paleomagnetism of mid-Cretaceous red beds in west-central Kyushu Island, southwest Japan: paleoposition of Cretaceous sedimentary basins along the eastern margin of Asia. Earth Planet. Sci. Lett. 201, 233–246.
Koike, T., 1996. The first occurrence of Griesbachian conodonts in Japan. Transaction and Proceedings of the Palaeontological Society of Japan, New Series 181, pp. 337–346.
Kopp, R.E., Kirschvink, J.L., 2008. The identification and biogeochemical interpretation of fossil magnetotactic bacteria. Earth Sci. Rev. 86, 42–61.
Lowrie, W., 1990. Identification of ferromagnetic minerals in a rock by coercivity and unblocking temperature properties. Geophys. Res. Lett. 17, 159–162.
Maloof, A.C., Kopp, R.E., Grotzinger, J.P., Fike, D.A., Bosak, T., Vali, H., Poussart, P.M., Weiss, B.P., Kirschvink, J.L., 2007. Sedimentary Iron Cycling and the Origin and Preservation of Magnetization in Platform Carbonate Muds, Andros Island, the Bahamas. Earth Planet. Sci. Lett. 259, 581–598.
McFadden, P.L., McElhinny, M.W., 1988. The combined analysis of remagnetization circles and direct observations in Paleomagnetism. Earth Planet. Sci. Lett. 87, 161–172.
McFadden, P.L., McElhinny, M.W., 1990. Classification of the reversal test in paleomagnetism. Geophys. J. Int. 103, 725–729.
Oda, H., Suzuki, H., 2000. Paleomagnetism of Triassic and Jurassic red bedded chert of the Inuyama area, central Japan. J. Geophys. Res. Solid Earth 105, 25743–25767.
Ogg, J.G., Ogg, G., Gradstein, F.M., 2008. Concise Geologic Time Scale. Cambridge University Press, Cambridge, U.K.
Opdyke, N.D., Roberts, J., Claoue-Long, J., Irving, E., Jones, P.J., 2000. Base of the Kiaman: its definition and global stratigraphic significance. Geol. Soc. Am. Bull. 112, 1315–1341.
Ota, A., Isozaki, Y., 2006. Fusuline biotic turnover across the Guadalupian–Lopingian (Middle–Upper Permian) boundary in mid-oceanic carbonate buildups: biostratigraphy of accreted limestone in Japan. J. Asian Earth Sci. 26, 353–368.
Passey, B.H., Henkes, G.A., 2012. Carbonate clumped isotope bond reordering and geospeedometry. Earth Planet. Sci. Lett. 351, 223–236.
Pullaiah, G., Irving, G., Buchan, K.L., Dunlop, D.J., 1975. Magnetization changes caused by burial and uplift. Earth Planet. Sci. Lett. 28, 133–143.
Ripperdan, R.L., 1990. Magnetostratigraphic investigations of the lower Paleozoic period boundaries, and associated paleogeographic implications. Geological & Planetary SciencesCalifornia Institute of Technology, Pasadena, California, p. 171.
Roberts, A.P., Florindo, F., Chang, L., Heslop, D., Jovane, L., Larrasoana, J.C., 2013. Magnetic properties of pelagic marine carbonates. Earth Sci. Rev. 127, 111–139.
Sano, H., Nakashima, K., 1997. Lowermost Triassic (Griesbachian) microbial bindstone-cementstone facies, southwest Japan. Facies 36, 1–24.
Seguin, M.K., Petryk, A.A., 1986. Paleomagnetic study of the Late Ordovician–Early Silurian platform sequence of Anticosti Island, Quebec. Can. J. Earth Sci. 23, 1880–1890.
Shen, S.Z., Mei, S.L., 2010. Lopingian (Late Permian) high-resolution conodont biostratigraphy in Iran with comparison to South China zonation. Geol. J. 45, 135–161.
Shen, S.Z., Henderson, C.M., Bowring, S.A., Cao, C.Q., Wang, Y., W., W., Zhang, H., Zhang, Y.C., Mu, L., 2010. High-resolution Lopingian (Late Permian) timescale of South China. Geol. J. 45, 122–134.
Shibuya, H., Sasajima, S., 1986. Paleomagnetism of red cherts — a case-study in the Inuyama area, central Japan. J. Geophys. Res. Solid Earth Planets 91, 14105–14116.

Stanley, S.M., Yang, X., 1994. A double mass extinction at the end of the Paleozoic era. Science 266, 1340–1344.
Steiner, M.B., 2006. The magnetic polarity time scale across the Permian–Triassic boundary. In: Lucas, S.G., Casinis, G., Schneider, J.W. (Eds.), Non-marine Permian biostratigraphy and biochronology. Geological Society of London, pp. 15–38.
Szurlies, M., 2013. Late Permian (Zechstein) magnetostratigraphy in Western and Central Europe. Geol. Soc. Lond. Spec. Publ. 376, 73–85.
Tobin, T.S., Ward, P.D., Steig, E.J., Olivero, E.B., Hilburn, I.A., Mitchell, R.N., Diamond, M.R., Raub, T.D., Kirschvink, J.L., 2012. Extinction patterns, delta(18) O trends, and magnetostratigraphy from a southern high-latitude Cretaceous–Paleogene section: links with Deccan volcanism. Palaeogeogr. Palaeoclimatol. Palaeoecol. 350, 180–188.
Uno, K., Onoue, T., Hamada, K., Hamami, S., 2012. Palaeomagnetism of Middle Triassic red bedded cherts from southwest Japan: equatorial palaeolatitude of primary magnetization and widespread secondary magnetization. Geophys. J. Int. 189, 1383–1398.
Vandervoo, R., 1990. The reliability of paleomagnetic data. Tectonophysics 184, 1–9.
Wang, Z.M., Vandervoo, R., Wang, Y.G., 1993. A new Mesozoic apparent polar wander loop for South China — Paleomagnetism of Middle Triassic rocks from Guizhou Province. Earth Planet. Sci. Lett. 115, 1–12.
Wang, W., Cao, C.Q., Wang, Y., 2004. The carbon isotope excursion on GSSP candidate section of Lopingian–Guadalupian boundary. Earth Planet. Sci. Lett. 220, 57–67.
Ward, P.D., Botha, J., Buick, R., De Kock, M.O., Erwin, D.H., Garrison, G.H., Kirschvink, J.L., Smith, R., 2005. Abrupt and gradual extinction among Late Permian land vertebrates in the Karoo Basin, South Africa. Science 307, 709–714.
Wardlaw, B.R., Davydov, V., Gradstein, F.M., 2004. The Permian period. In: Gradstein, F.M., Ogg, J.M., Smith, A.G. (Eds.), A Geologic Time Scale 2004. Cambridge University Press, Cambridge, pp. 249–270.
Watson, G.S., 1956. Analysis of dispersion on a sphere. Geophys. J. R. Astron. Soc. 7, 153–159.
Weiss, B.P., Baudenbacher, F.J., Wikswo, J.P., Kirschvink, J.L., 2001. Magnetic microscopy promises a leap in sensitivity and resolution. EOS Trans. Am. Geophys. Union 82, 513–518.
Yang, Z.Y., Besse, J., 2001. New Mesozoic apparent polar wander path for south China: tectonic consequences. J. Geophys. Res. Solid Earth 106, 8493–8520.
Yokoyama, M., Isozaki, Y., Otofuji, Y.-I., 2007. Rock magnetic study of the Middle to Late Permian shallow-sea limestones in the central Kyusyu. Japan Geoscience Union Meeting, Chiba City, Japan, p. E111-009.